Discrete rearranging disordered patterns: Prediction of elastic and plastic behavior, and application to two-dimensional foams

C. Raufaste[*]

*Laboratoire de Spectrométrie Physique, UMR 5588 CNRS and Université de Grenoble I, 140 Avenue de la physique,
BP 87, 38402 Saint Martin d'Hères, France
and Physics of Geological Processes, University of Oslo, P.O. Box 1048, Blindern, Oslo, Norway*

S. J. Cox

Institute of Mathematics and Physics, Aberystwyth University, Aberystwyth SY23 3BZ, United Kingdom

P. Marmottant

*Laboratoire de Spectrométrie Physique, UMR 5588 CNRS and Université de Grenoble I, 140 Avenue de la physique,
BP 87, 38402 Saint Martin d'Hères, France*

F. Graner

*Laboratoire de Spectrométrie Physique, UMR 5588 CNRS and Université de Grenoble I, 140 Avenue de la physique,
BP 87, 38402 Saint Martin d'Hères, France
and Institut Curie, BDD, UMR 3215 CNRS and Inserm U934, 26 rue d'Ulm, F-75248 Paris Cedex 05, France*

We study the elasto-plastic behavior of materials made of individual (discrete) objects such as a liquid foam made of bubbles. The evolution of positions and mutual arrangements of individual objects is taken into account through statistical quantities such as the elastic strain of the structure, the yield strain, and the yield function. The past history of the sample plays no explicit role except through its effect on these statistical quantities. They suffice to relate the discrete scale with the collective global scale. At this global scale, the material behaves as a continuous medium; it is described with tensors such as elastic strain, stress, and velocity gradient. We write the differential equations which predict their elastic and plastic behavior in both the general case and the case of simple shear. An overshoot in the shear strain or shear stress is interpreted as a rotation of the deformed structure, which is a purely tensorial effect that exists only if the yield strain is at least of order 0.3. We suggest practical applications including the following: when to choose a scalar formalism rather than a tensorial one; how to relax trapped stresses; and how to model materials with a low, or a high, yield strain.

I. INTRODUCTION

Discrete rearranging patterns include cellular patterns, for instance, liquid foams, biological tissues, and grains in polycrystals; assemblies of particles such as beads, granular materials, colloids, molecules, and atoms; and interconnected networks [1]. Many of these disordered materials display elastic and plastic properties, so that the stress tensor can rotate and is not necessarily aligned with the strain rate tensor; in models this effect is included in objective derivatives [2].

Use of simplified geometries, e.g., in a rheometer, allows a first characterization of the material through measurements of shear stress. An overshoot in the shear stress is seen during the first loading in materials such as polymers [3], granular materials [4], and emulsions [5]. For liquid foams this effect has been observed in a plate-plate rheometer [6] and in simulations [7,8]. It is unclear whether this is due to a change

in the material's structure or a tensorial effect of shear; but nevertheless the overshoot is an essential ingredient in a recent model [9] of the strain-rate discontinuity in the cylindrical Couette foam flow experiments of Ref. [10]. Such an overshoot results in mechanical bistability: two different values of strain correspond to the same value of stress between the plateau and the maximum and can thus coexist. Here, we investigate the elastic regime and elasto-plastic transition in a fully tensorial model. To describe the mechanical behavior we use a formalism adapted for discrete rearranging disordered patterns which enables us to quantify rotational effects and to test the relevant parameters [1].

We use as an example a sheared liquid foam [11–18]. Although a liquid foam consists only of gas bubbles surrounded by liquid walls, it exhibits a complex mechanical behavior. It is elastic for small strains, plastic for large strains, and flows at large strain rates [19–21]. This behavior is useful for numerous applications such as ore separation, oil extraction, foods, and cosmetics. The individual objects, namely, the bubbles, are easily identified, which makes a liquid foam (or alternatively an emulsion, made of droplets) a model for the study of other complex fluids.

This paper is organized as follows. In Sec. II, we simulate the quasistatic two-dimensional (2D) flow of a foam in a

_____

*Present address: Laboratoire de Physique de la Matière Condensée, UMR 6622 CNRS and Université de Nice-Sophia Antipolis, Parc Valrose, 06108 Nice Cedex 2, France; christophe.raufaste@unice.fr

Couette shear geometry; we explain how we perform and represent the measurements. In Sec. III, we present our equations and discuss the specific effects due to the use of tensors such as the overshoot. Section IV compares the model and the simulation and extracts the relevant information. Section V presents applications to practical situations, i.e., how and when to use the model. Section VI summarizes our findings. The Appendix explains the notation and provides the detailed equations.

II. SIMULATIONS

We simulate numerically a 2D foam flowing in a linear Couette shear geometry. Simulations of dry foams offer several advantages: (i) the parameters are homogeneous (liquid fraction, bubble area) and controlled (no diffusion-driven coarsening or film rupture); (ii) the yield strain is of order 0.3, which is large enough to observe a full tensorial elastic regime while small enough that plastic effects can be easily observed; (iii) all physical quantities can be easily measured.

A. Methods

Several ideal two-dimensional dry foams [19] are simulated (Fig. 1 and Table I). We use the SURFACE EVOLVER [23] in a mode in which each film is represented as a circular arc. The value of surface tension is taken equal to 1 throughout, without loss of generality. A realistic foam structure is found by minimizing the total film length subject to the constraint of fixed bubble areas prescribed at the beginning of the simulation. The simulations are quasistatic, which means that the system has time to relax between successive time steps (increments in applied strain). Relaxation effects are thus neglected and viscosity does not need to be included. The behavior is expected to be elasto-plastic.

The simulation procedure is as follows. A Voronoi construction of randomly distributed points [24] (not shown) is first used to generate a fully periodic tessellation of the plane. To create a confined foam, bubbles at the top and bottom are sequentially deleted until the required number of bubbles remains. In each case, the structure is imported into the SURFACE EVOLVER and target bubble areas prescribed, either all the same (monodisperse, $\delta A/A = 0$), a small random variation of up to 20% about monodisperse ($\delta A/A = 0.025$), or equal to the areas given by the Voronoi construction ($\delta A/A = 0.66$).

The initial foam configuration for each simulation [e.g., label (1) in Fig. 1] is found by reducing the total film length to a local minimum. During this minimization, neighbor swappings (so-called "T1s" [19]) are triggered by deleting each film that shrinks below a certain critical length l_c and allowing a new film to form to complete the process. The critical length l_c defines and measures an effective liquid fraction, Φ_{eff} [22], here chosen to be very dry (Table I).

One geometry consists of a unit cell of 400 bubbles with fully periodic boundary conditions to eliminate any artifacts due to small sample sizes. The second geometry mimics more closely a real experiment and consists of 296 bubbles with two parallel bars (about 15 bubble diameters apart) con-
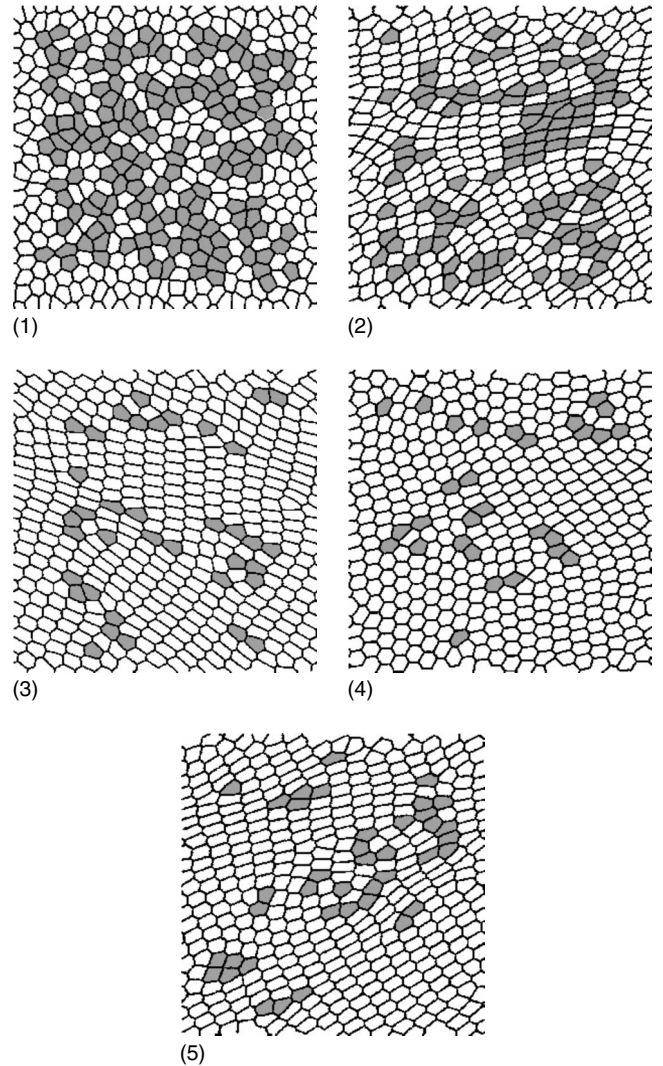

FIG. 1. Example of 2D foam simulation. Pictures are successive snapshots of a quasistatically sheared, fully periodic foam. Numbers correspond to those of Figs. 2 and 5. Bubbles with six neighbors are displayed in white, otherwise in gray.

fining the foam and with periodicity in one direction only.

To shear the foams, two different procedures are required. For the periodic foams, one off-diagonal component of the matrix describing the periodicity of the unit cell is adjusted

TABLE I. Characteristics of simulated foams. The different columns correspond to the symbols used in Figs. 8 and 10, effective liquid fraction [22], area dispersity, boundary conditions, and maximal amplitude of the cycles.

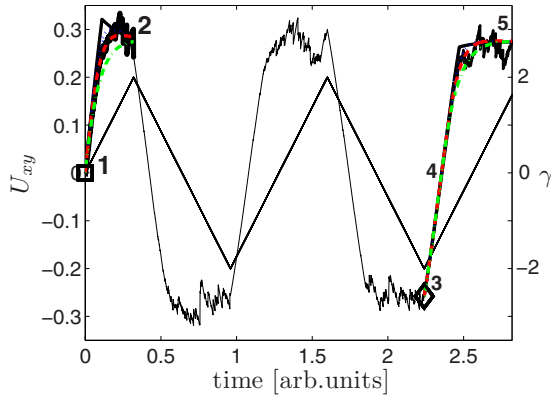| Symbol	Φ_{eff}	$\delta A/A$	Geometry	γ_{max}
▼ or ▽	9.7×10^{-5}	0	Fully periodic	± 2
× or +	3.9×10^{-4}	0	Fully periodic	± 2
◆ or ◇	3.9×10^{-4}	0.025	Fully periodic	± 2
▲ or △	3.9×10^{-4}	0.66	Fully periodic	± 2
● or ○	3.5×10^{-4}	0	Confined	± 2.5
■ or □	3.5×10^{-4}	0.66	Confined	± 2.5

FIG. 2. (Color online) Time evolution of the reference simulation (× in Table I). Horizontal axis: time is in arbitrary units, equivalent to the "cumulated strain" $\int |\dot{\gamma}| dt$, where t is the time and $\dot{\gamma}$ is defined up to an arbitrary prefactor; here 2.25 cycles are represented. Vertical axis: all curves represent U_{xy} (left scale) except for the sawtooth which is the applied γ (right scale). Numbers correspond to the pictures in Fig. 1. The first step, plotted with a thick solid line, starts at the □ (indicated also by a number 1) and its end is labeled by number 2: $\gamma = 0 \rightarrow 2$. The second step, plotted with a thin solid line, is from numbers 2 to 3. The third step, plotted with a middle solid line, starts at the ◇ (indicated also by a number 3) and extends to number 5: $\gamma = -2 \rightarrow 2$. Four predictions of the model are plotted as dashed lines (see Fig. 6 for explanation of the legend); for clarity they are plotted only from 1 to 2 and from 3 to 5: note that from 3 to 4 all predictions are indiscernible from the simulation.

by a small amount [23]. For the confined foams, a small step in strain is applied by moving one of the confining walls a small distance and then moving all vertices affinely. In each case this is followed by reduction in the film length to a minimum correct to 16 d.p. using a conjugate gradient (without biasing the search by introducing any large-scale perturbations of the structure).

Each foam is subjected to at least two "sawtooth" shear cycles of amplitude γ_{max}. Positive and negative steps correspond, respectively, to shear toward increasing or decreasing imposed strain γ (Fig. 2).

B. Measurements

At each step, the positions of the bubble centers and films are recorded. Tensorial quantities are measured by averaging over all bubbles as follows [1].

The texture tensor $\mathbf{M} = \langle \vec{\ell} \otimes \vec{\ell} \rangle$ is computed statistically as an average over vector links $\vec{\ell}$ between centers of neighboring bubbles. We assume here that the reference texture at rest, $\mathbf{M}_0$, is isotropic. We thus define it by measuring the average of the determinant of $\mathbf{M}$ over the duration of the whole simulation, $\det(\mathbf{M}_0) = \langle \det(\mathbf{M}) \rangle$. The elastic strain of bubbles expresses the deviation from the reference state, $\mathbf{U} = (\log \mathbf{M} - \log \mathbf{M}_0)/2$ [Eq. (A1c)].

This tensor is symmetric by construction ($U_{yx} = U_{xy}$); it can be diagonalized and has two eigenvalues (U_1, U_2) in two orthogonal eigendirections. The simulations [Fig. 3(a)] verify that we can reasonably assume its trace to be always close to
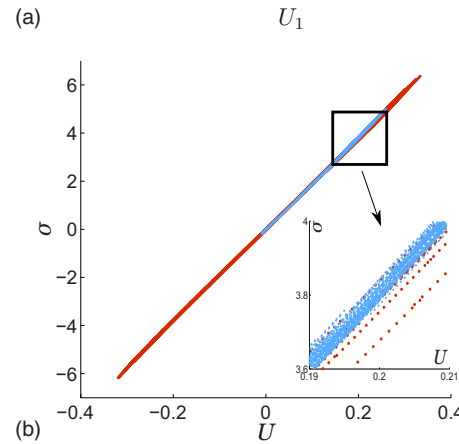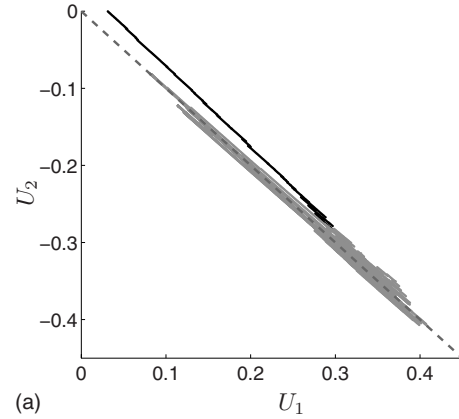

FIG. 3. (Color online) Validation of hypotheses. Both approximations of Sec. II B are tested during the shear of the reference simulation (× in Table I). (a) Strain eigenvalues U_1 vs U_2; black solid line: initial shear (1–2) which anneals the disorder; gray dots: shear cycles (2–5); dashed line: straight line of slope −1 passing through the origin. (b) Deviatoric stress-strain relation: dark red, σ_{xy} vs U_{xy}; light blue, $(\sigma_{xx} - \sigma_{yy})/2$ vs $(U_{xx} - U_{yy})/2$; red (dark) and blue (light) data almost perfectly overlap (see zoom in inset); the slope determines 2μ, where μ is the shear modulus.

zero, $U_1 + U_2 = U_{xx} + U_{yy} \approx 0$, as is roughly expected for an incompressible material [1]. Thus, due to its symmetry and vanishing trace, $\mathbf{U}$ has only two independent components:

$$\mathbf{U} = \begin{pmatrix} U_{xx} & U_{xy} \\ U_{yx} & U_{yy} \end{pmatrix} \approx \begin{pmatrix} \dfrac{U_{xx} - U_{yy}}{2} & U_{xy} \\ U_{xy} & -\dfrac{U_{xx} - U_{yy}}{2} \end{pmatrix}. \quad (1)$$

Figure 3(a) shows that our measurement of the elastic strain makes evident the effect of shear-induced shuffling [25]: the annealed foam (gray dots) differs significantly from the initial one (black solid line).

The contribution to the stress of the network of bubble walls is obtained by integrating over all films [26,27]; it yields the deviatoric (i.e., traceless) part of the elastic stress tensor σ. The trace of the stress, namely, the pressure, is unimportant here. The simulations are quasistatic and the viscous part of the stress is not relevant.

We check [Fig. 3(b)] that the stress and strain are strongly correlated; that their correlation is linear; and that it is iso-
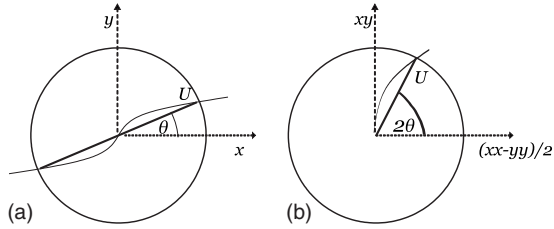
FIG. 4. Representation of the evolution of $\bar{\bar{U}}$. (a) Physical space: evolution of the point $(U\cos\theta, U\sin\theta)$; for completeness we also plot the opposite (and strictly equivalent) point $(-U\cos\theta, -U\sin\theta)$. (b) Component space: trajectory of $[(U_{xx}-U_{yy})/2, U_{xy}]$, that is, $(U\cos 2\theta, U\sin 2\theta)$.

tropic (the same for *xy* and *xx-yy* components) [28,29]. Half the slope thus defines and measures the elastic shear modulus μ.

C. Representations

To summarize, **M**, **U**, and σ characterize the current state of the foam. These three tensors carry here the same information, since μ appears constant. In what follows, texture, elastic strain, and stress tensors are always aligned.

We choose to display **U** only, because it is dimensionless, and thus more general: it makes the comparison of different materials easy. One possibility [1] is to represent the traceless tensor **U** as a circle of radius U, with a straight line to indicate the direction θ of its positive eigenvalue: see thick lines (circle and straight lines) in Fig. 4(a). We do not use it here, except in the inset of Fig. 8. In fact, it is easier to represent **U** at a given time by a point, enabling us to plot trajectories. Its two independent components can be represented in two different but equally useful ways, as follows. Both representations are equally appropriate in the problem considered here because of the circular symmetry of the yield criterion [see Eq. (5)].

First, in the case of a traceless tensor, the absolute value of the two eigenvalues is the same and equal to the amplitude U of the tensor **U** defined as

$$U = \sqrt{((U_{xx}-U_{yy})/2)^2 + U_{xy}^2}, \qquad (2)$$

or equivalently $U = |(U_1-U_2)/2| = \|\mathbf{U}\|/\sqrt{2}$, where $\|\mathbf{U}\| = [\Sigma_{ij}(U_{ij})^2]^{1/2}$ is the Euclidian norm of **U**. We call θ the direction of the greatest eigenvalue. We call *physical space* the representation of the parameters (U, θ). It is useful because it shows the evolution of the structure (elongation and orientation). In particular, we plot the trajectory of the point $[U\cos\theta(\gamma), U\sin\theta(\gamma)]$ [Fig. 4(a)].

The other representation, which has already been used for foams [8], is called *component space*. It plots the trajectory of the point $\{[U_{xx}(\gamma)-U_{yy}(\gamma)]/2, U_{xy}(\gamma)\}$ [Fig. 4(b)]. It is more suitable for comparison with experimental data, since rheometers measure the tangential stress (*xy*) and sometimes the normal stress difference (*xx-yy*).

These two possible choices are related by

$$U_{xy} = U\sin 2\theta, \qquad (3a)$$

$$\frac{U_{xx}-U_{yy}}{2} = U\cos 2\theta. \qquad (3b)$$

Complete data for one simulation are plotted in Fig. 5 and are discussed in the next section.

III. MODEL

A. Implementation

1. Elasticity equations

As already mentioned, we consider a quasistatic limit in which flow is slow enough that we may neglect viscous stresses. The stress is then related to the elastic strain [Fig. 3(b)]. We do not consider here the effect of external forces, such as gravity or friction on the boundary, if the system is confined between glass plates [16].

In the present 2D case, classical plasticity [30] suggests that the material begins to yield when the difference between the stress eigenvalues becomes too large: $(\sigma_1-\sigma_2)^2 = 4\sigma_Y^2$. The yield stress σ_Y separates a domain of pure elasticity from a domain in which the material flows plastically. A complete set of continuous equations (Reuss equations [30]) can then be derived; σ_Y is assumed to be constant (no strain hardening). The effect of pressure (trace of the stress) is neglected, which is usually a good first approximation for metals for instance [30]. It must be even more appropriate for soft materials, such as foam, for which the shear modulus is several orders of magnitude smaller than the bulk modulus [19]. In what follows we prefer to use the component yield criterion [30]:

$$\left(\frac{\sigma_{xx}-\sigma_{yy}}{2}\right)^2 + \sigma_{xy}^2 = \sigma_Y^2. \qquad (4)$$

Equivalently, Eq. (4) can be written for **U**, since the deviatoric parts of σ and **U** are proportional [Fig. 3(b)]. From Eqs. (2) and (4), we can write the yield criterion as

$$U = U_Y. \qquad (5)$$

This is represented by a circle in both physical and component spaces [Figs. 5(b) and 5(d)].

For the example of foams and highly concentrated emulsions, Marmottant and Graner [31] suggested that the transition between elastic and plastic regimes is not sharp, but can be described by a yield function h. This function is 0, respectively, 1, in the pure elastic, respectively, plastic, domain. Between these two limits, both effects are present and the proportion seems to depend mostly on the elastic strain amplitude U [Fig. 6(a)]. This assumption was successfully tested on different flow geometries of a 2D foam [29].

By assuming that the deformation is affine [1] and according to the prediction of plasticity (Eq. 22 in [29]), we can then write a tensorial equation of evolution of the texture (Eq. 9 in [1]). This dictates the evolution of the texture due to imposed strain (deformation and rotation) and due to relaxation (rearrangements); for details see Eqs. (A1d) and (A2):
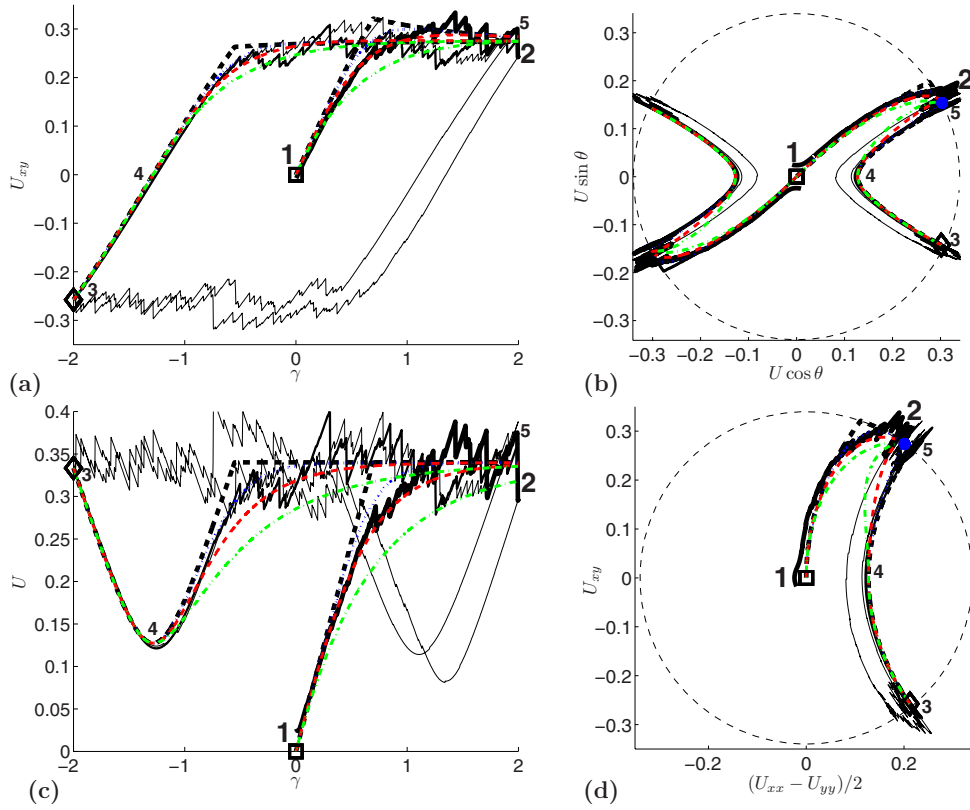
FIG. 5. (Color online) Different representations of Fig. 2 (same symbols) according to Fig. 4. (a) U_{xy} versus γ. (b) Physical space. (c) U versus γ. (d) Component space. The dashed circle in (b) and (d) has radius $U_Y = 0.34$.

$$\frac{d}{dt}\mathbf{M} = \mathbf{M} \cdot \nabla\mathbf{v} + \nabla\mathbf{v}^t \cdot \mathbf{M} - \left(\frac{\mathbf{U}}{U}{:}\nabla\mathbf{v}_{sym}\right)\mathcal{H}h\left(\frac{U}{U_Y}\right)\frac{\mathbf{U}}{U} \cdot \mathbf{M}.$$

(6)

Here d/dt is the Lagrangian derivative in time (including advection); $\mathbf{M} \cdot \nabla\mathbf{v} + \nabla\mathbf{v}^t \cdot \mathbf{M}$ is the variation in $\mathbf{M}$ due to convection by the velocity gradient $\nabla\mathbf{v}$; as explained in the Appendix, Secs. 1 and 3, the notation $U{:}\nabla\mathbf{v}_{sym}$ is the scalar product of the elastic strain tensor with the symmetrized velocity gradient tensor $\nabla\mathbf{v}_{sym} = (\nabla\mathbf{v} + \nabla\mathbf{v}^t)/2$ [1]; conversely, $\mathbf{U} \cdot \mathbf{M}$ is the usual product of tensors; here $\mathcal{H} = \mathcal{H}(\frac{\mathbf{U}}{U}{:}\nabla\mathbf{v}_{sym})$ is the Heaviside function, which is equal to 1 if $U{:}\nabla\mathbf{v}_{sym}$ is positive and 0 otherwise.

Equation (6) links the evolution of the foam texture with the elastic strain. It is quasistatic in the sense that the strain is relevant, not the strain rate. It can be generalized to evolutions quicker than the relaxation times of the structure [32]. Plasticity occurs only when the elastic strain is oriented in the direction of shear as expressed by the Heaviside function $\mathcal{H}$ (Appendix, Sec. 4).

The model is continuous and analytic, without fluctuations. The information regarding disorder is recorded in h. Trapped stresses [3] are recorded in the initial value $\mathbf{M}_i$ (or equivalently $\mathbf{U}_i$). The material's yielding criterion is encoded in U_Y. The history of the material only plays a role in determining h, $\mathbf{M}_i$ (or $\mathbf{U}_i$), and U_Y, which together fully describe the material. According to the expression for h, Eq. (6) can be integrated analytically or numerically.

2. Simple shear

To study the structure-evolution equation, i.e., the competition between elasticity and plasticity, and predict the rheological behavior, we impose a strain rate $\dot{\gamma}$ on the material. We take x as the direction of the shear, which gives the following velocity field:
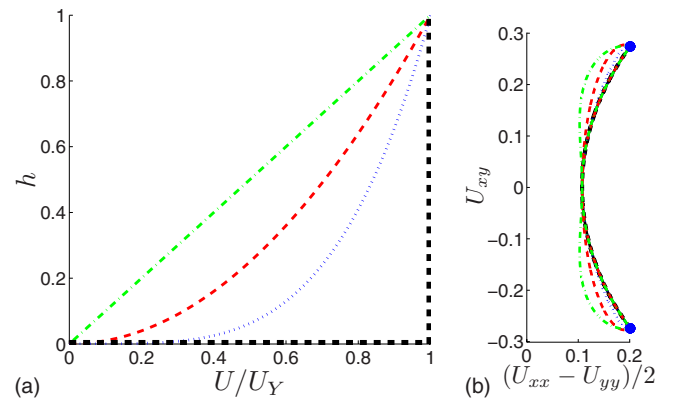

FIG. 6. (Color online) Model. (a) The different yield functions h used as examples in the present paper are power laws $h(U) = (U/U_Y)^n$ with $n = 1$ (green dashed dots), $n = 2$ (red dashes), $n = 4$ (blue dots), and $n = +\infty$ (black thick dashes; equal to 0 everywhere except at $U = U_Y$ where it is equal to 1). (b) Corresponding limit cycles predicted by the model plotted in component space (same legend).
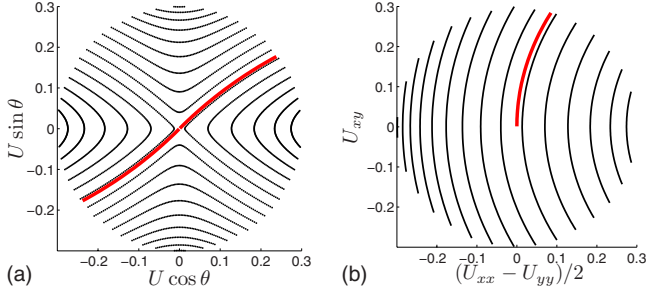
FIG. 7. (Color online) Elastic model represented in physical (a) and component (b) spaces. Different initial states are taken: $U_i = 0$ (center; red) and $U_i = 0.3$ (initial points scattered around the circle; black). Here $n \rightarrow +\infty$: all the trajectories evolve elastically. For $\dot{\gamma} > 0$, U_{xy} increases, that is, time evolves upward on (b). If $\dot{\gamma} < 0$, these graphs are unchanged, due to their symmetry with respect to the horizontal axis, showing that the purely elastic trajectories are reversible.

$$\nabla \mathbf{v} = \begin{pmatrix} \partial_x v_x & \partial_x v_y \\ \partial_y v_x & \partial_y v_y \end{pmatrix} = \dot{\gamma} \begin{pmatrix} 0 & 0 \\ 1 & 0 \end{pmatrix} \qquad (7)$$

and hence

$$\nabla \mathbf{v}_{sym} = \dot{\gamma} \begin{pmatrix} 0 & 1/2 \\ 1/2 & 0 \end{pmatrix}. \qquad (8)$$

This factor 1/2 appears when comparing the scalar and tensorial descriptions (Appendix, Sec. 5). In this geometry, the advection term is taken equal to zero and the resulting system of equations is given in the Appendix, Sec. 4. The reference state $\mathbf{M}_0$ is considered isotropic and constant throughout the evolution.

We recall that this evolution is quasistatic: $\dot{\gamma}$ appears as a prefactor in the time evolution, Eqs. (A3). We thus follow the evolution with the strain $\gamma = \int \dot{\gamma} dt$ instead of the time. Tensor operations and the time evolution of $\mathbf{M}$ are implemented by a finite difference procedure. Between two time steps, $\mathbf{U}$ is recalculated with Eq. (A1c).

B. Predictions

We now address the resolution of the full elasto-plastic set of equations (A3). Our representation underlines the specifically tensorial effects.

1. Purely elastic regime

As a first example of our representation, we consider here the pure elastic regime. This means that we allow the structure to deform elastically (stretching and contraction), but not to relax plastically (no rearrangements). Our formalism allows us to describe pure elasticity by computing the elastic strain and its evolution when the material is deformed. Our formalism extends to large strains, even those of order 1 (for strains much larger than 1, without plasticity, the formalism of large amplitude strain [33] might be preferable). Figures 7(a) and 7(b) show trajectories for different initial elastic strains.

For an initially isotropic material, $U_i = 0$, we recover the classical results in the small strain limit: $U \simeq \gamma/2$ and U_{xy}
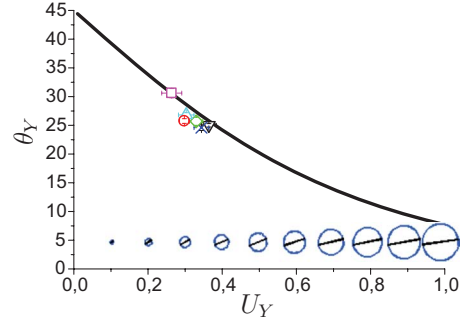

FIG. 8. (Color online) Plastic limit for $\dot{\gamma} > 0$. Model of θ_Y versus U_Y (solid line) and corresponding representations of $\mathbf{U}$ as circles with straight lines, indicating the direction of positive eigenvalue (inset), for several values of U_Y. Simulation points (same symbols as in Table I) are plotted for comparison.

$\simeq \gamma/2$. The Poynting relation [33] thus takes the form of a parabola; we even extend it to an initially anisotropic material, $U_i \neq 0$ [see Fig. 13 and Eq. (A16)]. For higher strains, U_{xy} is less linear with respect to γ due to the rotation of the elastic strain.

In all cases, U_{xy} increases monotonically. Note that this is not the case for $(U_{xx} - U_{yy})/2$ nor for U. When the structure is aligned perpendicularly to the shearing direction ($\mathbf{U}:\nabla\mathbf{v}_{sym} < 0$), it contracts ($U$ decreases) under shear until it aligns with the shear. When the structure is aligned parallel to the shearing direction ($\mathbf{U}:\nabla\mathbf{v}_{sym} > 0$), it stretches ($U$ increases) under shear. Since $\mathbf{U}$ is a tensor, it can continuously decrease, change direction, and increase again without ever vanishing (as opposed to a scalar, which can change sign only when it is equal to zero). For instance, a trajectory which starts with a direction opposed to that of shear has first a decreasing U (contraction, with U_{xy} negative and increasing), then an increasing U (stretching, with U_{xy} positive and increasing), then a constant U (yielding, with a rotation of $\mathbf{U}$ toward the plastic limit).

2. Plastic limit

The yield strain is the amplitude of the strain when the material yields, that is, a scalar number. The *plastic limit* is defined as the elastic strain tensor $\mathbf{U}$ obtained after an infinitely long shearing ($\gamma \rightarrow +\infty$). The amplitude of this tensor is that of the yield strain. Its direction is obtained by solving Eq. (6) when its left-hand side equals 0, h equals 1, and $\mathcal{H}$ equals 1:

$$U = U_Y, \qquad (9a)$$

$$\cos\theta = \frac{1}{\sqrt{1 + e^{-4U_Y}}}, \qquad (9b)$$

$$\sin\theta = \text{sign}(\dot{\gamma}) \frac{1}{\sqrt{e^{4U_Y} + 1}}. \qquad (9c)$$

This plastic limit is represented in Fig. 8. It shows that the larger U_Y, the less aligned $\mathbf{U}$ is with respect to $\nabla\mathbf{v}_{sym}$. This tensorial effect is strong because θ_Y decreases quickly with

U_Y. The scalar limit corresponds to $\theta \simeq 45°$ as discussed in Sec. V A.

3. Transient regime

We now consider the shearing of a material with initially anisotropic elastic strain, $\mathbf{U}_i \neq \mathbf{0}$. In *physical* or *component space*, the state of the material is initially situated on an elastic trajectory and must arrive at the plastic limit point [Figs. 9(a)–9(d)]. At this limit point, an increase in elastic strain is immediately transformed into plastic strain. Plasticity may occur only if $\mathbf{U} : \nabla \mathbf{v}_{sym} > 0$.

Graphically, both in physical space and in component space (Fig. 9), the plastic limit is represented by the point where a trajectory reaches perpendicularly the circle at $U = U_Y$ (the elastic strain increases along the tangent of the trajectory; the plastic strain relaxes toward the center of the circle: to balance each other, they must be parallel).

The shape of the yield function h then determines how the material reaches the plastic limit. For simplicity, we take h as a power-law function: $h = (U/U_Y)^n$ [Fig. 6(a)]. Two examples of the resulting behavior are plotted on Fig. 9. The limit $n \to \infty$ is intuitive: the material follows the elastic trajectory up to $U = U_Y$; then U is fixed and the plastic limit is reached by describing an arc of a circle in physical and component spaces [Figs. 9(a) and 9(b)]. For other cases (finite n) plasticity occurs earlier [Figs. 9(e) and 9(f)] and trajectories converge to the plastic limit [Figs. 9(c) and 9(d)].

The behavior changes qualitatively if the sign of $\dot{\gamma}$ is abruptly reversed. Unlike the elastic term, the plasticity term is irreversible due to the Heaviside function $\mathcal{H}$ in Eq. (6). This leads to an inversion of the plastic domain in physical and component spaces [Figs. 9(e) and 9(f)] and to a new plastic limit position [$\theta_Y \to -\theta_Y$; Eqs. (9)]. This hysteretic effect is shown in Fig. 5 by reversing $\dot{\gamma}$ once the plastic limit is reached. For high n, the new plastic limit is quickly reached, since the two plastic limits are on the same elastic trajectory.

If we perform alternate sign changes of $\dot{\gamma}$, we observe that the material is stuck in a limit trajectory [Fig. 6(b)]. This trajectory is almost insensitive to h and therefore close to the elastic trajectory joining the two plastic limits. This has an important consequence: once in the plastic regime, the elastic strain (and thus the stress) cannot be totally relaxed if we only reverse the shearing direction. This is examined in more detail below (Fig. 11).

4. Overshoot

As observed for $n \to +\infty$ [Fig. 9(b)], the overshoot is due to the transition from an elastic trajectory to the plastic limit. The structure itself has no overshoot: U increases monotonically. The overshoot appears in the tangential strain U_{xy}: it is a purely tensorial effect due to a rotation of the structure. In fact, U_{xy} increases in all elastic trajectories. Upon reaching $U = U_Y$ there is a sudden transition to the plastic regime. For trajectories to the left of the plastic limit [Fig. 9(b)], we see that U_{xy} decreases toward the plastic limit. The overshoot corresponds to the difference between the maximum value of U_{xy} (where the trajectory meets the circle) and the plateau value (plastic limit).
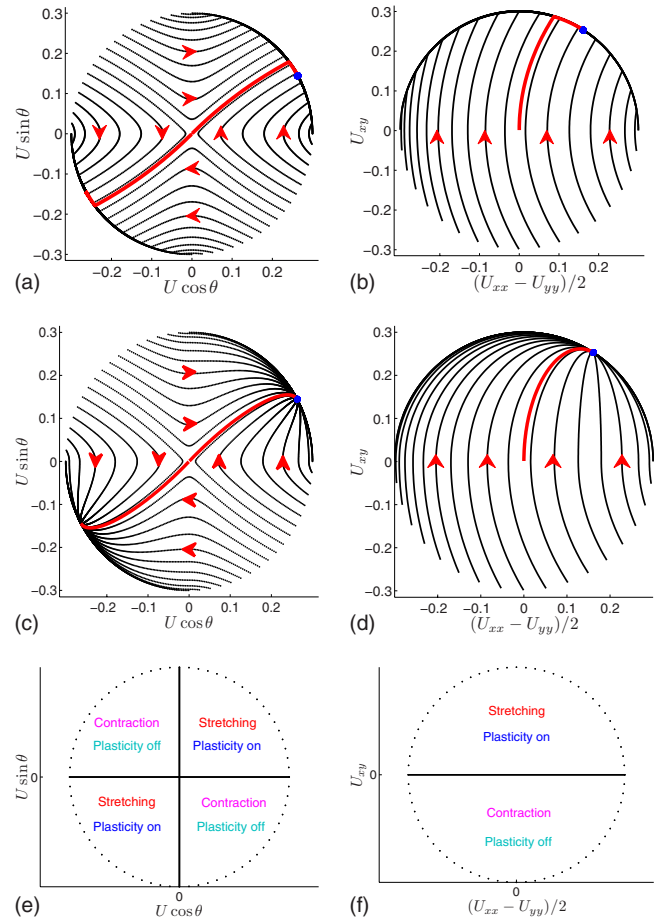

FIG. 9. (Color online) Elasto-plastic model. Representation of the model for $\dot{\gamma} > 0$ in physical [(a), (c), and (e)] and component [(b), (d), and (f)] spaces. If $\dot{\gamma} < 0$, the vertical axis of all these graphs should be inverted. [(a) and (b)] For $n \to +\infty$, all the trajectories evolve elastically (U_{xy} increases, that is, time evolves in the direction of the arrows) up to the yield strain, here taken as $U_Y = 0.3$, then evolve plastically (U constant) toward the plastic limit (blue point) which corresponds to a specific angle; see Eqs. (9). If the trajectory reaches the yield strain on the left of the plastic limit, U_{xy} passes through a maximum (overshoot). [(c) and (d)] For $n = 2$, plasticity appears more progressively, thus, smoothing the transition between elastic and plastic regimes and decreasing (or even suppressing) the overshoot. [(e) and (f)] Summary of the mechanical behavior: "stretching" and "contraction" according to the direction of $\mathbf{U}$ with respect to shear. Here "plasticity on" or "plasticity off" refers to the Heaviside function in the last term of Eq. (6), when the plasticity is progressive (n finite); when n increases the "plasticity on" zone narrows, and for n infinite it is reduced to the limit circle.

From Fig. 9(b), we observe a tiny overshoot for the normal stress difference if the trajectories reach the $U = U_Y$ circle to the right of the plastic limit. In that case, the trajectories move toward the right in the elastic regime, then toward the left in the plastic regime. Such trajectories correspond to the right of Fig. 9(b), that is, a structure with a large trapped normal stress difference $U_{xx} - U_{yy}$.

For smaller n, the elastic-plastic transition is smoother and the overshoot is reduced. The overshoot amplitude for different h and U_Y is plotted in Fig. 10 for the case of an

initially isotropic structure ($U_i = 0$). The overshoot increases with U_Y because the plastic limit moves away from the initial elastic trajectory.

IV. COMPARISON BETWEEN SIMULATIONS AND THE MODEL

A. Plastic limit

The model (Sec. III B 3) predicts that after a few cycles a limit trajectory is reached. This trajectory is also displayed in simulations by Kabla and Debregeas [8]. The plastic limit can thus be evaluated in simulations: U_Y is estimated by averaging U on the last plateau [using any of Figs. 5(a)–5(d)]; similarly, θ_Y is estimated by averaging θ on the last plateau of Fig. 5(b) or Fig. 5(d). In Fig. 8, results from simulations are compared with the model. The agreement is good and the model captures tensorial effects, especially because the measured θ_Y deviate much from the 45° scalar limit.

Taking larger l_c in the simulations favors neighbor swappings ("T1s"); thus, it corresponds to an increased effective liquid fraction. As expected [20,22], we see a decrease in U_Y. However, since the effective liquid fraction we are simulating remains in a very dry range ($< 4 \times 10^{-4}$), it does not influence much U_Y, which thus varies over a narrow range (0.26–0.37).

Reaching higher U_Y is possible with other materials, but not with disordered 2D foams. Reaching lower U_Y is possible (and usual) in experiments on disordered wet foams, but not in the present simulations where the algorithm would require adaptation at high l_c.

B. Yield strain and yield function

Simulation results fluctuate, due to the limited number of bubbles (discrete description), while model curves are smooth, corresponding to the limit of a large number of bubbles (continuous material description). There is a qualitative agreement, which is good enough to deduce U_Y and h approximately.

For instance, Fig. 5 compares a simulation with models using various h functions. We observe that $n \approx 2$ (red dashes in Fig. 5) describes well the simulation during the first positive shearing step, and $n \approx 4$ (blue dotted lines in Fig. 5) during the second one. Similarly, U_Y is deduced from the plateau value of U (Figs. 8 and 10).

In practice, in a first approximation, it is enough to consider U_Y and h as constant. Their variations are small and thus have a small effect on the foam rheology. However, these variations do exist.

For instance, in this example of Fig. 5, n (and thus h) evolves throughout the simulation revealing that the structure evolves too; h seems to be sensitive to the (topological) disorder of the foam [25]. Here U_Y is constant, but there are other cases (data not shown; see [34]) where, due to the decrease in the topological disorder during the shearing, U_Y decreases.

More generally, a real foam is constantly evolving under the effect of drainage, coarsening [21], or shuffling [25].

These effects should probably be considered in future models, which would try to predict U_Y and h, based on the average and fluctuations of the structure, respectively.

C. Overshoot

We can now identify two distinct physical mechanisms which can cause a stress overshoot in shear experiments of elasto-plastic materials. The first one is an *orientation* effect suggested in Sec. III B 4. U increases monotonically, but if U_Y is large enough then the rotation of **U** under shear implies that the tangential shear strain U_{xy} passes through a maximum. This purely tensorial effect is absent from scalar models. Under certain additional conditions on the initial elastic strain U_i, which are also described correctly only when taking into account the tensorial aspects, the normal strain difference $U_{xx} - U_{yy}$ also passes through a maximum.

Figure 10 shows a comparison between the model and the simulations. Given that in the range of simulated U_Y the overshoot is tiny and difficult to extract from the fluctuations, the agreement is surprisingly good. In most foam experiments, where U_Y is even lower, this effect should be too small to be measurable.

The second mechanism is outside of the scope of the present paper. It is due to an evolution of the *structure* itself during the first shear step (see Sec. IV B). This might be invoked to explain the larger overshoot of the data corresponding to the confined simulations (last simulations in Table I), as well as most experimental observations (such as that of Ref. [6]).

V. PRACTICAL APPLICATIONS

A. Comparison between scalar and tensorial representations

As long as the applied shear keeps a constant direction, and the elastic strain remains much smaller than 1, its eigenvectors correspond to that of $\nabla \mathbf{v}_{sym}$. That is, they are at 45° to the direction of shear. This is called the *scalar approximation* and it considerably simplifies the study of the mechanical behavior. In that case, a single (scalar) number is enough to fully describe the elastic strain.

This scalar number can equally well be chosen as the amplitude U, or the eigenvalue U_1, or the tangential shear strain U_{xy}, among others. To switch from one choice to the other requires care regarding the prefactors [29]: this is often a source of confusion in the literature, especially regarding the definition and value of the yield strain. The link between the simplified (scalar) and complete (tensorial) equations is detailed in the Appendix, Sec. 5, using $2U_{xy}$ as a scalar.

If $U_Y \ll 1$, which is the case for wet foams and emulsions, then U remains always much smaller than 1, and $\theta_Y \simeq 45°$, so that the scalar approximation holds; see Fig. 19 in Ref. [29] (except if the direction of the shear changes, in 2D or in 3D). In that limit tensorial effects such as normal differences or stress overshoot are negligible.

Quantitatively, U_{xy} is linked to $\sin(2\theta)$ [Eq. (3a)]. This implies that a difference of 10% between the scalar and tensorial equations is reached when $\sin(2\theta_Y) = 0.9$, which corresponds to $U_Y = 0.23$ [Eqs. (9)]. Very dry foams, such as those
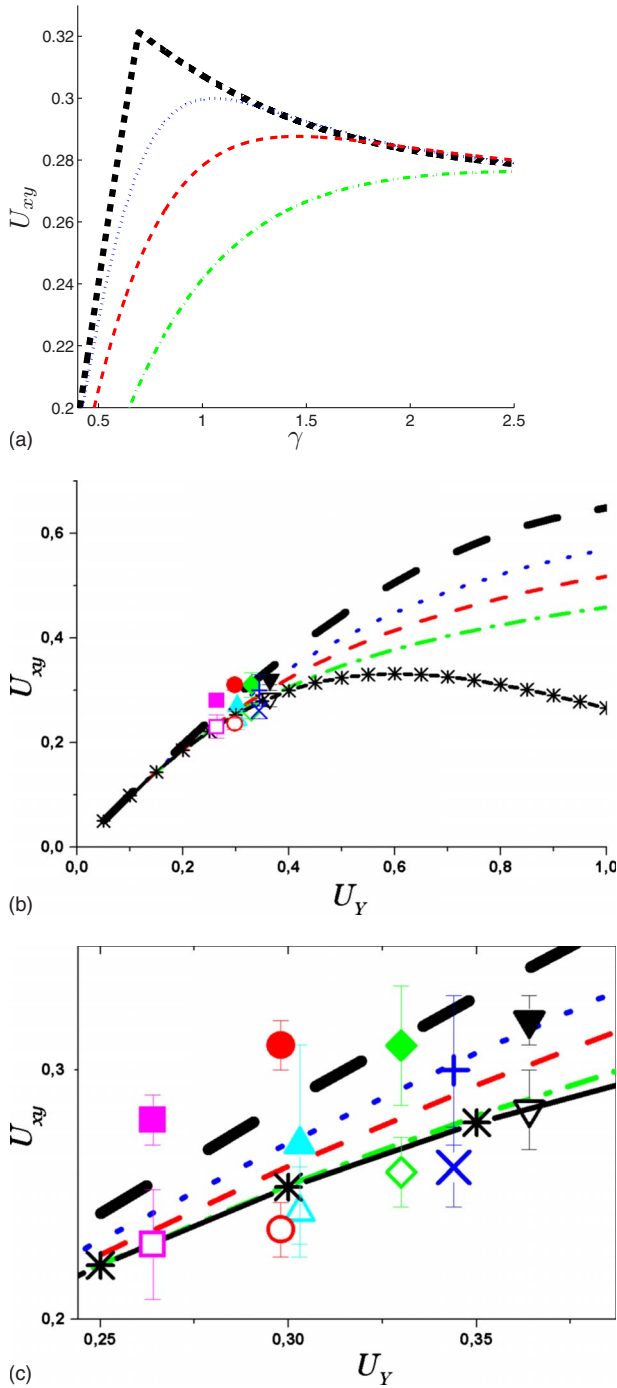
(a)

(b)

(c)

FIG. 10. (Color online) Overshoot, defined as the difference between the maximum of the U_{xy} versus γ curve, and the value of the plateau which follows this maximum. Calculations are performed in the case of an initially isotropic structure ($U_i=0$). (a) Zoom over the maxima of the curves of Fig. 5(a). (b) Maxima for different h functions (same legend as Fig. 6), and plateau value (starred line, which is the same for all h functions), plotted vs U_Y. Simulation points are plotted for comparison, with the same symbols as in Table I; closed symbols and + correspond to the maximal value (averaged over a few successive points) during the first shear step; open symbols and × correspond to the averaged value along the plateau of the last shear step; U_Y is measured as the plateau value of U. (c) Zoom of (b).

(a)

(b)
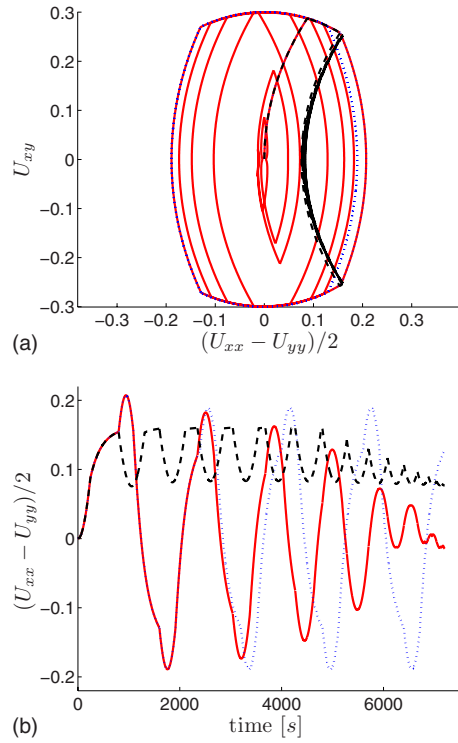
FIG. 11. (Color online) Shearing cycles to remove trapped stresses. Here $U_i=0$ for the first step and $U_Y=0.3$, $n\to+\infty$. Between two steps: the direction of shearing is turned 90° clockwise (blue dots); the amplitude is decreased from $\gamma=2$ to 0 in 15 steps (black dashes); simultaneously, the direction of shear is turned and its amplitude is decreased (red solid line). (a) Component space. (b) $(U_{xx}-U_{yy})/2$ versus time ($|\dot{\gamma}|=2.5\times10^{-3}$ s^{-1}).

simulated here, are slightly above this limit: a tensorial model is therefore useful.

B. Trapped strains and stresses

A dry foam is a material with sufficiently high U_Y that normal stresses may exist even when the material is at rest [3,15,35]. To relax such residual (or "trapped") stresses, we should first shear the foam enough to reach the plastic stage, so that plastic rearrangements anneal the disorder. We then must perform cycles of shear.

If the direction of shear is kept constant, and the shear simply reversed, the foam asymptotically reaches a limit trajectory, and the stress is not relaxed. Decreasing the amplitude of the shear cycle does not enable the foam to leave this limit trajectory [black dashes in Figs. 11(a) and 11(b)]. Kraynik *et al.* simulated dry 3D foam and applied shearing cycles (actually uniaxial contractions) of amplitude ≈0.2 in different directions rotated by 90°; this procedure decreases the trapped stress by a factor of around 2, which does not improve with more cycles (Fig. 7 of [35]).

Here we propose a reproducible procedure based on Sec. III B 3, which couples shearing cycles in different directions and decreasing amplitudes as follows:

(i) The amplitude γ_i of the first step is large enough to completely reach the plastic stage: $\gamma_i \gg 2U_Y$.
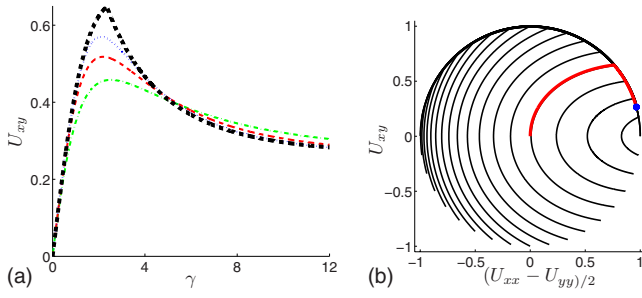
FIG. 12. (Color online) Representations of the model for U_Y $=1$. (a) U_{xy} versus γ for the first step and different yield functions, as in Fig. 6(a). (b) Representation of the model for $\dot{\gamma}>0$ in component spaces for $n\to+\infty$, as in Fig. 9(b).

(ii) At each step, the shearing direction is rotated by 90° and the shearing amplitude is decreased.

(iii) The decrease in amplitude between successive steps is smaller than $2U_Y/5$ ensuring there are at least five steps between $2U_Y$ and 0 (i.e., the total number of steps is at least $5\gamma_i/2U_Y$).

The red solid line in Figs. 11(a) and 11(b) shows that the normal stress difference decreases more at each cycle; for instance, six cycles yield a decrease by a factor of 10, apparently without saturating. In 3D the procedure is the same, rotating the shearing direction successively along the x, y, and z axes [35]. This procedure is easy to apply to simulations especially of fully periodic foams. In experiments, a special setup should be built: in 2D, it can be a rubber frame in the spirit of Refs. [11,25], if the four corners can be independently displaced.

C. Materials with low and high U_Y

For practical purposes we plot the reference curves for two limiting types of materials: those with U_Y much higher or much lower than 0.23. Figure 12 shows the example of $U_Y=1$. The plastic limit corresponds to a small angle θ_Y resulting in a strong overshoot.

Figure 13 shows that for small strains in the elastic regime, all curves can be expressed using a single parameter; for instance, as here, U_n^i, which is the normal elastic strain $U_n=(U_{xx}-U_{yy})/2$ at zero tangential shear ($U_{xy}^i=0$). A rough parabolic approximation and a refined one [Eq. (A16)] are plotted here for $U_Y=0.3$. For smaller U_Y, this approximation
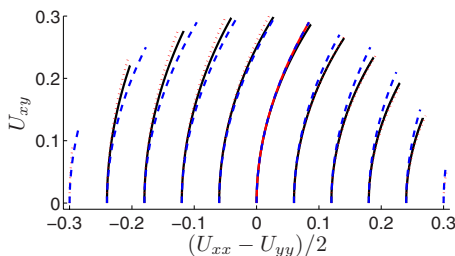

FIG. 13. (Color online) Representations of the model for small strains. U_{xy} vs $U_n=(U_{xx}-U_{yy})/2$. Black solid line: exact model. Blue dashes: first parabolic approximation $U_n=U_n^i+U_{xy}^2$. Red dots: complete parabolic approximation [Eq. (A16)].

is good over its whole range of validity (namely, the elastic regime), but this range is smaller.

VI. SUMMARY

We propose a continuous model of the elasticity and plasticity of disordered, discrete materials such as cellular patterns (for instance, liquid foams or emulsions) and assemblies of particles (for instance, colloids). It is based on statistical quantities including (i) the elastic strain **U**, a dimensionless quantity measurable on images, which facilitates the comparison between different experiments or models and makes apparent the effect of shear on the material's structure; (ii) the yield strain U, a classical criterion for the transition between reversible, elastic, and irreversible plastic regimes; (iii) and the yield function $h(U/U_Y)$, which describes how progressive this transition is by measuring the relative proportion of elastic and plastic deformation. They suffice to relate the discrete scale with the collective global scale. At this global scale, the material behaves as a continuous medium; it is described with tensors such as strain, stress, and velocity gradient. We give the differential equations which predict the elastic and plastic behavior. The model is fully tensorial and thus general, in 2D or in 3D.

We study in detail the case of simple shear. An original representation, suitable for 2D incompressible materials, is introduced to follow the evolution of the material during shear.

Since **U** is a tensor, it has an orientation and an amplitude, which both evolve under shear. It can continuously decrease its amplitude, change direction, and increase again its amplitude without ever vanishing (as opposed to a scalar, which can change sign only when it is equal to zero). Predictions of the model regarding orientation and stretching are plotted. They include a rotation of the structure, which can induce an overshoot of the shear strain or shear stress (and a smaller, rarer overshoot in normal stress differences) even without overshoot in the elastic strain amplitude. This purely tensorial effect exists if U_Y is at least of order 0.3. Independently, the shear can also induce a change in the material's structure, sometimes resulting in a (purely scalar) overshoot in the modulus of the elastic strain.

The model extends a classical plasticity criterion to disordered media. It can be solved numerically and yields testable predictions. We successfully compare them with carefully converged quasistatic simulations of shear cycles in 2D foams: the elastic strain increases, saturates, and reverses. From this comparison between model and simulation we determine U_Y and estimate h. This method is similar to that which we have used in experiments to extract U_Y [18,29] and a rough estimate of h. We still lack a model to predict U_Y and h. Both quantities evolve throughout the simulation, probably due to the evolution of the foam's internal structure, as well as the disorder and fluctuations. In short, the material obeys a continuous description determined by its average properties, while U_Y and h account for the effect at large scale of its fluctuations.

All quantities involved in the model are directly measurable, as tensors, in the current state of the material; this in-

cludes trapped stresses which we discuss (we also explain how to relax them): the history of the sample which led to this current state plays no other direct explicit role. We explain how and when to use the model in practice and provide a set of curves and analytical approximations including a discussion and an extension of the Poynting relation. At low strain, typically below 0.2, tensorial effects vanish and an approximate scalar simplification holds.

APPENDIX: DETAILED EQUATIONS

1. Notation for tensors

We collect here a list of our notation, since the definitions are scattered throughout the text. For a symmetric tensor $\mathbf{A}$, we denote by A_1 and A_2 its eigenvalues, by $A_1 + A_2 = A_{xx} + A_{yy}$ its trace, by $A_{xy} = A_{yx}$ its off-diagonal term, by $A_n = (A_{xx} - A_{yy})/2$ half its normal difference, by $A = \sqrt{((A_{xx} - A_{yy})/2)^2 + A_{xy}^2}$ its amplitude, and by $\|\mathbf{A}\| = A\sqrt{2}$ its Euclidian norm defined as $\|\mathbf{A}\|^2 = \mathbf{A} : \mathbf{A}$. The scalar product of two tensors $\mathbf{A}$ and $\mathbf{B}$ is defined as $\mathbf{A} : \mathbf{B} = \sum_{ij} A_{ij} B_{ij}$.

For a traceless tensor, $A_1 = -A_2 > 0$. If θ is the angle corresponding to A_1, then the point with coordinates $(A \cos \theta, A \sin \theta)$ is a representation of the actual direction of the tensor (*physical space*). Conversely, the point with coordinates $A_n = A \cos 2\theta$ and $A_{xy} = A \sin 2\theta$ directly represents the components of the tensor (*component space*). For a tensor, θ is defined modulo π (and not 2π as for vectors), so that 2θ has usually more relevance than θ. Similarly, for traceless tensors with eigendirections making a relative angle ϕ, their scalar product is proportional to $\cos 2\phi$. This scalar product is maximal when the two eigenvectors of the positive eigenvalues coincide, and minimized when they are perpendicular.

2. Complete system of equations

We have obtained [34] a complete (closed) set of equations:

$$\rho \frac{d}{dt}\vec{v} = \nabla \cdot (-p\mathbf{Id} + 2\mu\mathbf{U}), \tag{A1a}$$

$$\mathrm{div}\ \vec{v} = 0, \tag{A1b}$$

$$\mathbf{U} = \frac{1}{2}(\log \mathbf{M} - \log \mathbf{M}_0), \tag{A1c}$$

$$\frac{d}{dt}\mathbf{M} = \mathbf{M} \cdot \nabla \mathbf{v} + \nabla \mathbf{v}^t \cdot \mathbf{M} - 2\mathbf{P} \cdot \mathbf{M}. \tag{A1d}$$

Equation (A1a) is the equation of dynamics, equivalent to Navier-Stokes, except that here the viscous stress is assumed to be negligible compared to the elastic stress. Equation (A1b) assumes that the flow is incompressible; this assumption is often valid for foams at small deformation but can be relaxed if needed. Equation (A1c) defines the elastic strain from the texture [1], that is, it assumes that each bubble's internal degrees of freedom depend on its shape. Equation (A1d) is the evolution of the texture; see Eq. (6) for the definitions of its terms (transport and source). Here the plasticity rate $\mathbf{P}$ is predicted according to Eq. 22 in Ref. [29]:

$$\mathbf{P} = \frac{1}{2}\left(\frac{\mathbf{U}}{U} : \nabla \mathbf{v}_{sym}\right)\mathcal{H}\left(\frac{\mathbf{U}}{U} : \nabla \mathbf{v}_{sym}\right)h\left(\frac{U}{U_Y}\right)\frac{\mathbf{U}}{U}. \tag{A2}$$

The meaning of each term is the following. The direction of $\mathbf{P}$ is set by that of $\mathbf{U}$ indicating that the plasticity is opposed to the increase in $\mathbf{U}$. The amplitude of $\mathbf{P}$, which is the rate of plastic rearrangements, is the inverse of time. It is determined by the total strain rate $\nabla \mathbf{v}_{sym}$; more precisely, by one component of $\nabla \mathbf{v}_{sym}$ determined by the scalar product with $\mathbf{U}$ (and only if this scalar product is positive, as expressed by the Heaviside function $\mathcal{H}$). Finally, the amplitude of $\mathbf{P}$ depends on the yield criterion as expressed by $h(U/U_Y)$: the plasticity appears (progressively or abruptly) when U approaches then exceeds the yield strain.

Equation (A2) is written here by assuming that $\mathbf{M}$ and $\mathbf{U}$ commute (see Eq. 20 of Ref. [1]), which is always the case if $\mathbf{M}_0$ is isotropic. Like Eq. (A1b), it assumes that the flow is incompressible, but can be extended to more general cases. It also assumes that the flow is slow: see ref [31]. for a discussion of "quasistatic" flow, and [18,32] for the extension to higher velocity. The next sections examine more restrictive cases, that is, additional approximations: simple shear (Appendix, Sec. 3), small strain (Appendix, Sec. 5), and the purely elastic regime (Appendix, Sec. 6).

3. Simple shear

In our geometry, the notation becomes

$$\nabla \mathbf{v}_{sym} = \frac{\dot{\gamma}}{2}\begin{pmatrix} 0 & 1 \\ 1 & 0 \end{pmatrix},$$

$$\mathbf{M} = \begin{pmatrix} M_{xx} & M_{xy} \\ M_{xy} & M_{yy} \end{pmatrix},$$

$$\mathbf{U} = \begin{pmatrix} U_{xx} & U_{xy} \\ U_{xy} & U_{yy} \end{pmatrix},$$

$$\mathbf{U} : \nabla \mathbf{v}_{sym} = U_{xy}\dot{\gamma} = U\dot{\gamma}\sin 2\theta.$$

Here, due to our conventions, the angle between both tensors is $\phi = \theta - 45°$, hence the term $\cos 2(\theta - 45°) = \sin 2\theta$. This

scalar product is maximal when the two eigenvectors of the positive eigenvalues coincide (which happens for $\theta = 45°$), and minimized when they are perpendicular ($\theta = 90°$).

4. Elasto-plastic component equations

Under simple shear the advection term is supposed equal to zero and Eq. (A1d) becomes

$$\frac{1}{\dot{\gamma}} \partial_t M_{xx} = 2M_{xy} - \frac{U_{xy}}{U^2} \mathcal{H}(\dot{\gamma} U_{xy}) h\left(\frac{U}{U_Y}\right) [\bar{\bar{U}} \cdot \bar{\bar{M}}]_{xx},$$

(A3a)

$$\frac{1}{\dot{\gamma}} \partial_t M_{yy} = - \frac{U_{xy}}{U^2} \mathcal{H}(\dot{\gamma} U_{xy}) h\left(\frac{U}{U_Y}\right) [\bar{\bar{U}} \cdot \bar{\bar{M}}]_{yy}, \quad \text{(A3b)}$$

$$\frac{1}{\dot{\gamma}} \partial_t M_{xy} = M_{yy} - \frac{U_{xy}}{U^2} \mathcal{H}(\dot{\gamma} U_{xy}) h\left(\frac{U}{U_Y}\right) [\bar{\bar{U}} \cdot \bar{\bar{M}}]_{xy}. \quad \text{(A3c)}$$

The elastic regime can be studied by taking the last term of these equations equal to 0 (limit of high U_Y). The plastic limit is calculated by taking the left-hand sides of these equations equal to 0, $h = 1$, and $\mathcal{H} = 1$.

5. Scalar limit

In the limit of small strain, **U** can be linearized:

$$\mathbf{U} = \frac{1}{2\lambda_0} (\mathbf{M} - \mathbf{M}_0),$$

(A4)

where λ_0 is the isotropic eigenvalue of $\mathbf{M}_0$. In that limit Eq. (A3c) becomes

$$\frac{1}{\dot{\gamma}} \partial_t U_{xy} = \left(U_{yy} + \frac{1}{2} \right) - \frac{1}{2} \left(\frac{U_{xy}}{U} \right)^2 \mathcal{H}(\dot{\gamma} U_{xy}) h\left(\frac{U}{U_Y}\right). \quad \text{(A5)}$$

Assuming that θ remains close to 45° leads to

$$U_{xx} = U_{yy} = 0,$$ (A6a)

$$|U_{xy}| = U,$$ (A6b)

$$\partial_t 2 U_{xy} = \dot{\gamma} - \dot{\gamma} \mathcal{H}(\dot{\gamma} U_{xy}) h\left(\frac{|U_{xy}|}{U_Y}\right). \quad \text{(A6c)}$$

The last equation is identified as the scalar elasto-plastic equation [31], by taking $2 U_{xy}$ as the scalar elastic strain.

6. Analytical approximation at small strain

In a purely elastic regime, the evolution equation for the texture is

$$M_{yy} = M_{yy}^i,$$

$$M_{xy} = M_{yy}^i \gamma + M_{xy}^i,$$ (A7)

$$M_{xx} = M_{yy}^i \gamma^2 + 2 M_{xy}^i \gamma + M_{xx}^i.$$

To express all curves analytically, we choose a single parameter, for instance, the elastic strain in a nonsheared state ($U_{xy}^i = M_{xy}^i = 0$):

$$M_n = M_n^i + \frac{M_{yy}^i}{2} \gamma^2,$$ (A8)

$$M_{xy} = M_{yy}^i \gamma,$$ (A9)

which can be rewritten by eliminating γ:

$$M_n = M_n^i + \frac{M_{xy}^2}{2 M_{yy}^i}.$$ (A10)

There are still two constants left, M_n^i and M_{yy}^i. To eliminate one of them, we use the fact that the trace of **U** is almost zero, and thus the determinant of **M** is almost constant:

$$M_{xx}^i M_{yy}^i = \lambda_0^2,$$ (A11)

or equivalently, using Eq. (A10):

$$(2 M_n^i + M_{yy}^i) M_{yy}^i = \lambda_0^2.$$ (A12)

Solving Eq. (A12) yields

$$\frac{M_{yy}^i}{\lambda_0} = - \frac{M_n^i}{\lambda_0} + \sqrt{\left(\frac{M_n^i}{\lambda_0} \right)^2 + 1}$$ (A13)

or equivalently, eliminating M_{yy}^i using Eq. (A12):

$$M_n = M_n^i + \left[\sqrt{\left(\frac{M_n^i}{\lambda_0} \right)^2 + 1} + \frac{M_n^i}{\lambda_0} \right] \frac{M_{xy}^2}{2\lambda_0}. \quad \text{(A14)}$$

Coming back to **U** using Eq. (A4):

$$U_{xy} = \frac{1}{2\lambda_0} M_{xy}, \quad U_n = \frac{1}{2\lambda_0} M_n.$$ (A15)

Equation (A14) yields a parabolic approximation:

$$U_n = U_n^i + \left[\sqrt{\left(\frac{U_n^i}{\lambda_0} \right)^2 + 1} + \frac{U_n^i}{\lambda_0} \right] U_{xy}^2. \quad \text{(A16)}$$

The parameter which determines each elasticity curve is the normal strain difference at zero shear (which is thus equal to the amplitude of elastic strain at zero shear). Equation (A16) is tested on Fig. 13 for U up to 0.3. The prefactor of the parabola, i.e., the bracketed expression in Eq. (A16), is exactly 1 if $U_n^i = 0$: this is the Poynting relation [33] (black solid curve in Fig. 13, starting from the point $U_n = U_{xy} = 0$). In fact, even for $U_n^i \neq 0$, the bracket in Eq. (A16) remains close to 1: as shown in Fig. 13, the Poynting relation extends even to an initially anisotropic material.

[1] F. Graner, B. Dollet, C. Raufaste, and P. Marmottant, Eur. Phys. J. E **25**, 349 (2008).

[2] D. Kolymbas and I. Herle, Int. J. Numer. Analyt. Meth. Geomech. **27**, 733 (2003).

[3] R. G. Larson, *The Structure and Rheology of Complex Fluids* (Oxford University Press, New York, 1999).

[4] N. Xu and C. S. O'Hern, Phys. Rev. E **73**, 061303 (2006).

[5] S. T. Lahtinen, Acta Aliment. **17**, 219 (1988).

[6] S. A. Khan, C. A. Schnepper, and R. C. Armstrong, J. Rheol. **32**, 69 (1988).

[7] T. Okuzono and K. Kawasaki, Phys. Rev. E **51**, 1246 (1995).

[8] A. Kabla and G. Debregeas, J. Fluid Mech. **587**, 23 (2007).

[9] D. Weaire, R. J. Clancy, and S. Hutzler, e-print arXiv:0907.1624.

[10] J. Lauridsen, G. Chanan, and M. Dennin, Phys. Rev. Lett. **93**, 018303 (2004).

[11] A. Abd el Kader and J. C. Earnshaw, Phys. Rev. Lett. **82**, 2610 (1999).

[12] G. Debrégeas, H. Tabuteau, and J.-M. di Meglio, Phys. Rev. Lett. **87**, 178305 (2001).

[13] J. Lauridsen, M. Twardos, and M. Dennin, Phys. Rev. Lett. **89**, 098303 (2002).

[14] E. Pratt and M. Dennin, Phys. Rev. E **67**, 051402 (2003).

[15] E. Janiaud and F. Graner, J. Fluid Mech. **532**, 243 (2005).

[16] Y. Wang, K. Krishan, and M. Dennin, Phys. Rev. E **73**, 031401 (2006).

[17] E. Janiaud, D. Weaire, and S. Hutzler, Phys. Rev. Lett. **97**, 038302 (2006).

[18] I. Cheddadi, P. Saramito, C. Raufaste, P. Marmottant, and F. Graner, Eur. Phys. J. E **27**, 123 (2008).

[19] D. Weaire and S. Hutzler, *The Physics of Foams* (Oxford University Press, Oxford, 1999).

[20] A. Saint-Jalmes and D. J. Durian, J. Rheol. **43**, 1411 (1999).

[21] R. Höhler and S. Cohen-Addad, J. Phys.: Condens. Matter **17**, R1041 (2005).

[22] C. Raufaste, S. Cox, B. Dollet, F. Graner, and Y. Jiang, Eur. Phys. J. E **23**, 217 (2007).

[23] K. Brakke, Exp. Math. **1**, 141 (1992).

[24] K. Brakke, 200,000,000 Random Voronoi Polygons, www.susqu.edu/brakke/papers/voronoi.htm (unpublished).

[25] C. Quilliet, S. Ataei Talebi, D. Rabaud, J. Käfer, S. J. Cox, and F. Graner, Philos. Mag. Lett. **88**, 651 (2008).

[26] G. K. Batchelor, J. Fluid Mech. **41**, 545 (1970).

[27] S. J. Cox and E. L. Whittick, Eur. Phys. J. E **21**, 49 (2006).

[28] M. Asipauskas, M. Aubouy, J. A. Glazier, F. Graner, and Y. Jiang, Granular Matter **5**, 71 (2003).

[29] P. Marmottant, C. Raufaste, and F. Graner, Eur. Phys. J. E **25**, 371 (2008).

[30] R. Hill, *The Mathematical Theory of Plasticity* (Clarendon, Oxford, 1950).

[31] P. Marmottant and F. Graner, Eur. Phys. J. E **23**, 337 (2007).

[32] P. Saramito, J. Non-Newtonian Fluid Mech. **145**, 1 (2007).

[33] V. Labiausse, R. Höhler, and S. Cohen-Addad, J. Rheol. **51**, 479 (2007).

[34] C. Raufaste, Ph.D. thesis, Université Grenoble I, 2007 (http://tel.archives-ouvertes.fr/tel-00193248/en/).

[35] A. M. Kraynik, D. A. Reinelt, and F. van Swol, Phys. Rev. E **67**, 031403 (2003).